Voprosy Onkologii = Problems in Oncology. 2025. Vol. 71, № 6
UDC 615.849-006
DOI 10.37469/0507-3758-2025-71-6-OF-2310

© *Ivan A. Kurnosov[1], Pavel V. Balakhnin[1], Dmitry A. Gulyaev[1,2,3], Darya R. Subbotina[1], Vasilii I. Malkevich[1], Anastasia L. Muravtseva[1], Aleksei S. Shmelev[1], Vladislav Yu. Chirkin[2], Ilya A. Burovik[1], Sergey S. Bagnenko[1,4], Alexey M. Belyaev[1,3]*

Flat-Detector Computed Tomography: Advancing Real-Time Neuronavigation for Stereotactic Brain Tumor Biopsy

[1]N.N. Petrov National Medical Research Center of Oncology, St. Petersburg, the Russian Federation
[2]Almazov National Medical Research Center, St. Petersburg, the Russian Federation
[3]North-Western State Medical University named after I.I. Mechnikov, St. Petersburg, the Russian Federation
[4]St. Petersburg State Pediatric Medical University, St. Petersburg, the Russian Federation

Introduction. Stereotactic brain tumor biopsy (STB) currently relies on two primary navigation technologies: frame-based and frameless systems. A significant limitation of both approaches is the inability to visualize the target tumor and biopsy needle in real-time during needle insertion.

Aim. To evaluate the technical efficacy, safety, advantages, and limitations of performing STB under real-time flat-panel detector computed tomography (FDCT) guidance.

Materials and Methods. Between December 2021 and December 2024, 99 patients (46 men, 53 women; median age 56 [46; 68] years) underwent FDCT-guided STB. Procedures were performed using an Artis Zee Floor angiographic system (Siemens, Germany) equipped with a 16-bit digital detector (40 × 30 cm) and utilizing various contrast enhancement techniques. The acquired FDCT images were analyzed using the standard InSpace software package, and trajectory planning was conducted with the iGuide Needle Guidance application. Biopsy needle insertion was performed under two-projection laser guidance and augmented fluoroscopy control. Post-procedural FDCT scans were obtained to confirm technical success and diagnose potential complications.

Results. The median target tumor volume was 6.9 [2.4; 16.6] ml, with a median targeting path length of 47.5 [38; 56] mm. Histological material was successfully obtained in 98% of cases, yielding diagnoses of 62 gliomas, 25 lymphomas, 5 demyelinating processes, 3 encephalitis cases, one adenocarcinoma metastasis of unknown primary, and one case of Erdheim-Chester disease. The median procedure duration was 53 [43; 65] minutes. Complications occurred in 3 (3%) patients, including two cases of intracranial hemorrhage (promptly diagnosed and managed during the procedure) and one case of persistent neurological deficit. No mortality was recorded.

Conclusion. This study demonstrates high diagnostic efficacy and safety of FDCT-guided STB. This technique overcomes the principal limitations of frame-based and frameless STB by providing reliable intraoperative trajectory planning, high-quality real-time neuroimaging and neuronavigation, and immediate complication detection with potential for timely intervention.

Keywords: stereotactic biopsy of brain tumors; neuroimaging; neuronavigation; flat-detector computed tomography; FDCT

For Citation: Ivan A. Kurnosov, Pavel V. Balakhnin, Dmitry A. Gulyaev, Darya R. Subbotina, Vasilii I. Malkevich, Anastasia L. Muravtseva, Aleksei S. Shmelev, Vladislav Yu. Chirkin, Ilya A. Burovik, Sergey S. Bagnenko, Alexey M. Belyaev. Flat-detector computed tomography: Advancing real-time neuronavigation for stereotactic brain tumor biopsy. *Voprosy Onkologii = Problems in Oncology.* 2025; 71(6): 00-00.-DOI: 10.37469/0507-3758-2025-71-6-OF-2310

✉ Contacts: Ivan A. Kurnosov, ivkurnosov@gmail.com

Introduction

Biopsy followed by histological and molecular-genetic analysis plays a key role in the diagnosis and treatment of primary brain tumors such as astrocytomas, gliomas [1], lymphomas [2], and others. This surgical procedure may be required to determine the molecular-genetic profile of intracranial metastases in cases of cancer of unknown primary, isolated metastatic brain involvement, synchronous multiple primary cancer, as well as to select targeted therapy [3]. The optimal material for histological examination is tumor tissue removed during radical open (or endoscopic) surgery; however, the indications for such procedures are limited to solitary, resectable intraparenchymal (or intraventricular) lesions [1]. In cases of deeply located tumors (basal ganglia, brainstem, etc.), lesions in eloquent areas (motor cortex, etc.), suspected lymphomas, as well as multifocal or diffusely infiltrative growth, tissue sampling is most commonly performed using stereotactic (needle) biopsy (STB) [1–3].

At present, two types of navigational neurosurgical technologies are widely used for STB — frame-based stereotactic navigation (with Leksell frames (Elekta, Stockholm, Sweden) and Cosman-Roberts-Wells frames (Radionics, Burlington, USA) and frameless navigation based on optical tracking systems (Stealthstation (Medtronic, Dublin, Ireland) and Brainlab (Brainlab, Munich, Germany) [4–6].

The main drawback of both technologies is that needle advancement within the brain and tissue sampling are performed without direct visual control. Therefore, it is practically impossible during the procedure to assess the precise position of the needle either within the tumor or relative to critical brain structures [1]. Brain shift due to cerebrospinal fluid leakage (after opening the dura mater) or nee-

dle deflection during advancement is not captured or displayed on the monitors with either frame-based or frameless navigation [1]. During the biopsy, it is also nearly impossible to identify potential complications such as off-target sampling of normal brain, sampling of necrotic tumor (non-diagnostic biopsy), as well as the development of hemorrhage in the form of intratumoral bleeding, intraventricular hematoma, or blood oozing along the biopsy track [1, 7]. To confirm on-target sampling and to diagnose/exclude complications, the anesthetized patient must be transported to the radiology suite for an additional scan, which is impractical in routine clinical practice [1].

The principal complications of STB are a non-diagnostic tissue sample that fails to verify the tumor and necessitates repeat intervention, and clinically significant intratumoral hemorrhage at the sampling site [7, 8]. A recently published meta-analysis comparing frame-based and frameless biopsies of brain tumors larger than 10 mm found no statistically significant differences in diagnostic yield (from 84.0 to 100 % and from 86.6 to 100 %, respectively), the rate of clinically significant hemorrhage (from 5.1 to 14.2 % and from 2.4 to 17.8 %, respectively), the frequency of permanent neurological deficit (from 2.8 to 13.9 % and from 1.3 to 15.4 %, respectively), or mortality (from 1.2 to 3.9 % and from 1.3 to 3.6 %, respectively) between the two navigational technologies [4]. At the same time, it is known that the effectiveness of STB directly depends on tumor size and depth. Accordingly, both technologies show markedly lower diagnostic accuracy (and higher complication rates) when sampling lesions smaller than 10 mm in diameter (i.e., < 1 mL), as well as tumors with areas of necrosis or intratumoral hemorrhage, resulting in verification in no more than 60–70 % of cases [1]. Numerous adjunct techniques have been proposed to increase the informational value of biopsy material (such as intraoperative cytological assessment, intraoperative frozen-section analysis, Raman spectroscopy, fluorescence microscopy, fluorescence confocal microscopy, multiphoton microscopy, mass spectrometry, etc.), as well as to reduce the risk of intratumoral bleeding (trans-needle endoscopic fluorescence, laser Doppler flowmetry, optical coherence tomography, controlled negative-pressure aspiration, etc.) [3]. Robotic targeting systems have also been developed to improve accuracy for small lesions [8]. However, all these developments only modestly affect technical outcomes and complication rates, because their use does not eliminate the inherent limitations of frame-based and frameless navigation [1]. Another serious drawback of both navigational technologies is the absolute dependence of operating neurosurgeons on the radiology department, for which such invasive procedures are, by definition, not a priority. Equipping neurosurgical operating rooms with cross-sectional imaging systems (multidetector computed tomography (MDCT) and/or magnetic resonance imaging (MRI)) is extremely costly and cannot fundamentally change the situation, as these modalities are designed primarily for neuroimaging rather than for three-dimensional real-time neuronavigation [9].

Thus, there is a pressing need to develop new, more reliable and practical real-time neuroimaging and neuronavigation technologies capable of improving workflow and the technical effectiveness of STB for brain tumors, as well as enhancing safety [7]. For these purposes, the use of flat-panel detector computed tomography (FDCT) [10], integrated into modern angiography suites [11], appears optimal. FDCT imaging capabilities are currently widely used in neuroradiological endovascular procedures [12]. At the same time, the application of FDCT-based neuroimaging and the considerable potential of percutaneous FDCT-guided navigation technologies (augmented fluoroscopy) [13] for transcranial interventions is, at present, essentially limited to placement of external ventricular drains in subarachnoid hemorrhage [14, 15] and drainage of spontaneous intracerebral hematomas [16].

An analysis of studies indexed in the PubMed and RSCI electronic medical databases as of March 15, 2025, identified, according to the specified search criteria, only a single publication from our group devoted to this method [19]. No other reports describing clinical use of FDCT imaging and FDCT navigation technologies for STB of brain tumors were found. The aim of study is to evaluate the technical effectiveness, safety, advantages, and limitations of performing stereotactic biopsy (STB) of brain tumors under real-time flat-panel detector computed tomography (FDCT) guidance.

Materials and Methods

Within a prospective observational study, all stereotactic brain tumor biopsy procedures were performed under real-time FDCT — guidance. The decision to proceed with intervention was made at a multidisciplinary tumor board including a neurosurgeon, medical oncologist, radiologist, radiation oncologist, and an interventional radiologist. All patients underwent comprehensive clinical and diagnostic work-up that mandatorily included brain MRI with intravenous bolus contrast; in 13 patients, positron emission tomography–computed tomography (PET/CT) with ^{11}C-methionine or ^{18}F-fluoroethyltyrosine was also performed. Indications for STB were suspected unresectable primary brain tumors (astrocytomas, oligodendrogliomas, etc.) or primary central nervous system lymphoma of any size. Prior to STB, written informed consent

for the intervention and for subsequent data processing and use was obtained from all patients.

Primary data were collected and systematized using Microsoft Office Excel 2016, and statistical analysis was performed in STATISTICA 12 (StatSoft). On initial analysis, the Shapiro–Wilk test yielded $p < 0.05$ for most variables, indicating deviation from normality; therefore, nonparametric methods were applied. Associations between quantitative variables were assessed with Spearman's rank correlation, and group comparisons were performed using the Mann–Whitney U test. Statistical significance was set at $p < 0.05$. Quantitative data are presented as the median (Me) with the first and third quartiles (Q1–Q3).

From December 2021 to December 2024, STB was performed in 99 patients (46 men and 53 women). The median age was 56 (46; 68) years.

Target lesion laterality was right hemisphere in 53 patients, left in 38, and corpus callosum in 8. By location, tumors were parietal in 31 patients, frontal in 28, basal ganglia in 11, posterior corpus callosum in 8, temporal in 7, occipital in 5, thalamic in 4, cerebellar in 3, and insular in 2.

In 23 cases, a guiding platform was installed after creating a 14-mm burr hole. In the remaining 76 procedures, a freehand technique was used; in 8 of these, a minimally invasive 2.2-mm twist-drill burr hole was created.

All STB procedures were performed in the interventional radiology operating suite (angiography suite) on an Artis Zee Floor system (Siemens, Munich, Germany) equipped with a flat-panel 16-bit digital detector measuring 40 × 30 cm. Operations were carried out by one of two neurosurgeons with 7 and 8 years of experience, respectively, together with one of two interventional radiologists with 8 and 24 years of experience, respectively. In all cases, a 2.1-mm side-cut (10-mm) MDT Medtronic Navigated Biopsy Needle (Medtronic, Dublin, Ireland) was used.

Within the first 24 hours after STB, control MDCT was performed; in the absence of life-threatening complications, patients were transferred from the intensive care unit to the neurosurgery department. Discharge occurred on postoperative days 4–5.

Data analysis included correlation of variables such as patient age and sex, contrast-enhancement pattern, and target tumor volume and location. We also analyzed discrepancies between preoperative diagnostic MRI and intraoperative FDCT with respect to the size and structure of targeted lesions; the access formation method and use of a guiding platform; brain shift after dural opening; targeting tract length and deviation from the planned trajectory; number of needle passes; number of FDCT scans; number of tissue cores obtained and total operative time; the number, types, severity, and timing of complications; histological diagnosis; diagnostic yield of the biopsy; and length of hospital stay.

Description of the original FDCT-guided STB technique

In the initial stage of method development, in patients whose tumors did not enhance on diagnostic MRI, STB was performed under FDCT guidance without additional contrast administration. FDCT was acquired in the 10sDCT Head mode, after which the resulting data were fused with diagnostic MRI (T2-FLAIR or T1+C) or PET/CT using the 3D/3D Fusion software package (Siemens, Munich, Germany). Visualization of the target lesion (from which tissue sampling was planned) and navigation were performed exclusively according to MRI or PET/CT data (fig. 1, A), while the subsequent steps of the procedure did not differ from those described below. In patients with contrast-enhancing tumors on diagnostic MRI at the initial stage of the method, intraprocedural imaging employed intravenous contrast enhancement consisting of slow (manual)

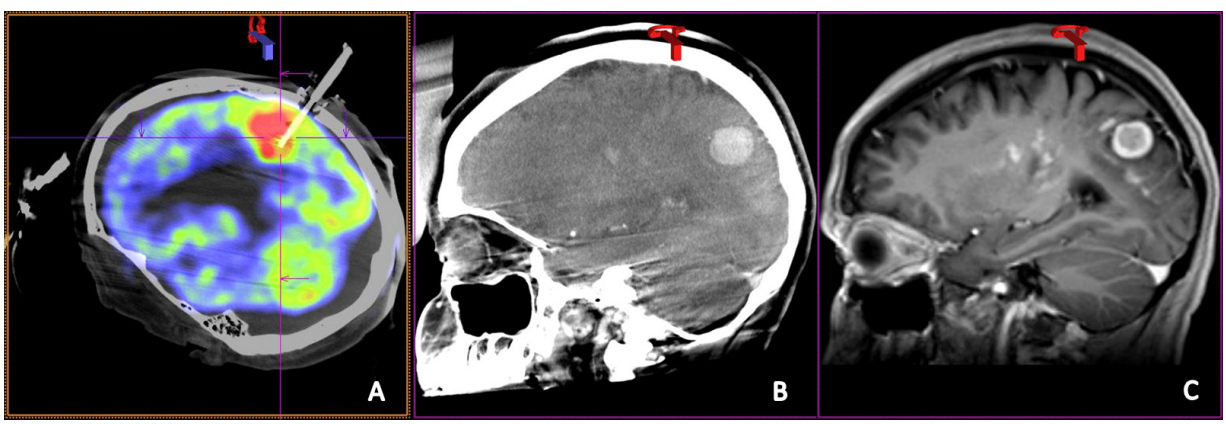

Fig. 1. A. Stereotactic brain tumor biopsy (STB) using fusion of two imaging datasets: intraprocedural non-contrast FDCT and 11C-methionine PET-CT. The stage of biopsy needle position verification within the tumor is shown. B. Visualization of primary brain lymphoma using intraprocedural FDCT with intravenous contrast enhancement (interstitial phase). C. Preoperative MRI with multiphase intravenous contrast (T1-weighted) of the same patient

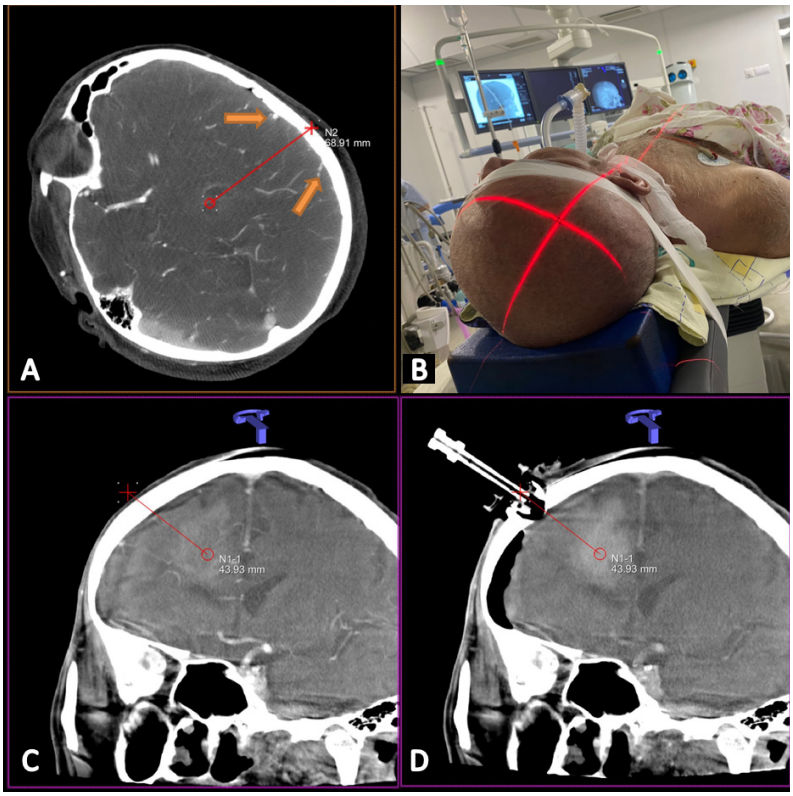

Fig. 2. A. Planning tumor targeting trajectories using intraoperative FDCT with multiphase intravenous bolus contrast. The stage of determining the trajectory's proximal point, accounting for the location of cortical veins (orange arrows) and arteries along the entire route (arteriovenous phase of FDCT contrast), is shown. B. Laser guidance, a standard feature of the angiographic unit, indicates the entry point on the patient's scalp (via a laser crosshair) according to the planned tumor targeting trajectory. C-D. Significant displacement of brain tissue and target tumor (relevant for targeting) after dural opening in a patient with severe replacement hydrocephalus. Images show the parenchymal phase of FDCT with intravenous multiphase bolus contrast before access (C) and the interstitial phase of FDCT after burr hole creation and guide pad placement (D)

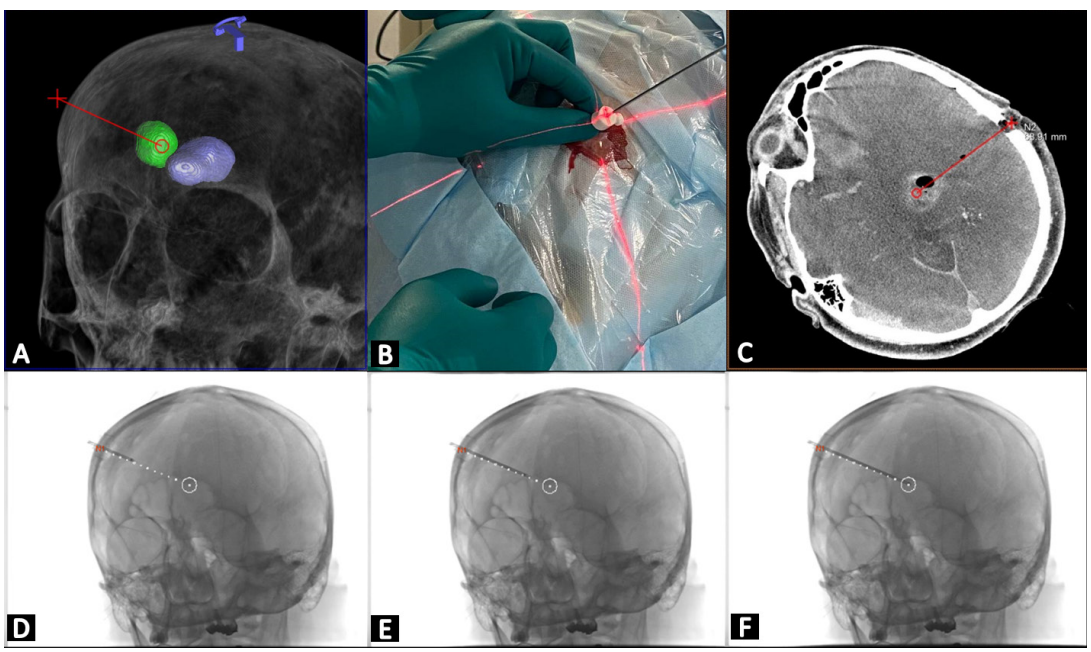

Fig. 3. A. Planning of the tumor targeting trajectory with its segmentation in a three-dimensional stereotaxic space (colored green) with simultaneous visualization of the adjacent right lateral ventricle (purple), penetration of which must be avoided during biopsy sampling; B. The process of determining the exact targeting direction using a guiding pad and a laser guidance system. With the correct positioning of the pad, the needle shaft should be illuminated by a laser along its entire length in two orthogonal projections; C. Control FDCT without additional contrast after performing a biopsy and removing the biopsy needle. An air bubble is visualized at the site of sampling of biopsy material from the tumor (brain lymphoma). No data were obtained for intratumor hemorrhage, blood leakage through the puncture channel, displacement of brain structures, or the formation of a hematoma at the access site; D–F. Stages of advancing the biopsy needle to the target point using the augmented fluoroscopy mode (augmented reality). On the fluoroscopic monitor, in one of two mutually perpendicular projections, the advancing needle is visualized in real time, according to the previously planned targeting trajectory, which is also reflected on the monitor. For more accurate advancing of the needle in three-dimensional space, the C-arm must be periodically transferred to the second orthogonal projection, also using fluoroscopic control

injection of 70–100 mL of iodinated contrast medium (Iopromide, Ultravist-370, Bayer, Germany) into a peripheral vein 3–5 minutes before the first FDCT scan (fig. 1, B–C). When visualization quality was insufficient, FDCT data were also fused with MRI and/or PET/CT.

Subsequently, as the method evolved, tumor visualization predominantly used a multiphasic intravenous bolus FDCT-contrast protocol. The overall algorithm for STB was as follows. After induction of general anesthesia on the angiography table, the patient's head was secured with sterile adhesive tape in a position optimal for neurosurgical access. Through a peripheral venous catheter and using a Mark 7 Arterion syringe-injector (Bayer Medrad, Leverkusen, Germany), 9 mL of contrast was injected at 3 mL/s and digital subtraction angiography was performed at 1 frame/s to determine the exact onset of opacification of the common carotid arteries. Next, biphasic FDCT of the brain was performed during intravenous bolus administration of 90 mL of contrast at 3 mL/s (30-s injection) using the same injector. The first scan (arteriovenous phase) was started 10 seconds after the onset of carotid opacification (i.e., 20–30 seconds from the start of injection) and acquired over 20 seconds in the 20sDCT Head mode; the second, identical, scan was started 10 seconds after completion of the first (50–60 seconds from the start of injection — parenchymal phase). Data sets were reconstructed on a Syngo X-Workplace VD10E (Siemens, Munich, Germany) workstation in automatic mode using a 512 × 512 matrix without smoothing. Image analysis was performed in InSpace (Siemens, Munich, Germany) in MPR and MIP modes, and targeting trajectories were planned with the iGuide Needle Guidance package (Siemens, Munich, Germany). The optimal needle trajectory was determined using both contrast phases merged into a single data set via 3D/3D Fusion. For the first (distal) point (the planned start of stepwise tissue sampling), the safest area of viable tumor with clear enhancement on the parenchymal-phase FDCT was chosen, while avoiding regions containing large tumor vessels on the arteriovenous-phase FDCT. The second (proximal) trajectory point was set based on the arteriovenous-phase data so that the path traversed a cortical gyrus, bypassed sulci and cortical veins, and simultaneously avoided white-matter tracts, ventricles, arteries, veins, and choroid plexuses along the entire planned biopsy tract (fig. 2, A). In some cases, in addition to intraoperative FDCT data, diagnostic MRI and/or PET/CT were also used in fusion mode. After trajectory planning, its coordinates were transferred into the stereotactic space of the angiography system, and the angiographic table and C-arm were aligned to the specified direction with a "top-view" position. Upon coordinate registration, a laser crosshair automatically illuminated the exact scalp entry point and enabled determination of attack angles (fig. 2, B). A burr hole was then made and the dura opened. At the early stages of the method and in cases with challenging trajectories, a guiding platform from the Medtronic navigated biopsy needle kit (Medtronic, Dublin, Ireland) was additionally fixed to the skull. After access formation, a repeat FDCT scan was mandatory (hereafter also in 20sDCT Head mode), corresponding to the interstitial phase of enhancement. Using these data, as well as the prior phases available via 3D/3D Fusion, the targeting trajectory was adjusted taking into account the burr-hole position and any brain shift after dural opening (fig. 2, C–D). The target tumor was then segmented, and the boundaries of critical structures adjacent to the trajectory were delineated (fig. 3, A). Under laser guidance illuminating two mutually perpendicular planes along the needle shaft, the needle was advanced into the target using a freehand technique. Needle advancement within brain structures was also monitored using augmented fluoroscopy available in two orthogonal projections (fig. 3, D–E). This technology allowed real-time visualization of the needle itself and (in virtual space and not in real time) the premarked trajectory, segmented target, arteries, and veins. When a guiding platform was used, its working position was set under fluoroscopy in the top-view position, after which the needle was advanced along the prescribed path (fig. 3, B). Otherwise, the procedure did not differ from the freehand technique. After reaching the target point — mandatorily confirmed by fluoroscopy in two orthogonal projections — multilevel stepwise sampling of tumor tissue was performed, aiming to obtain at least

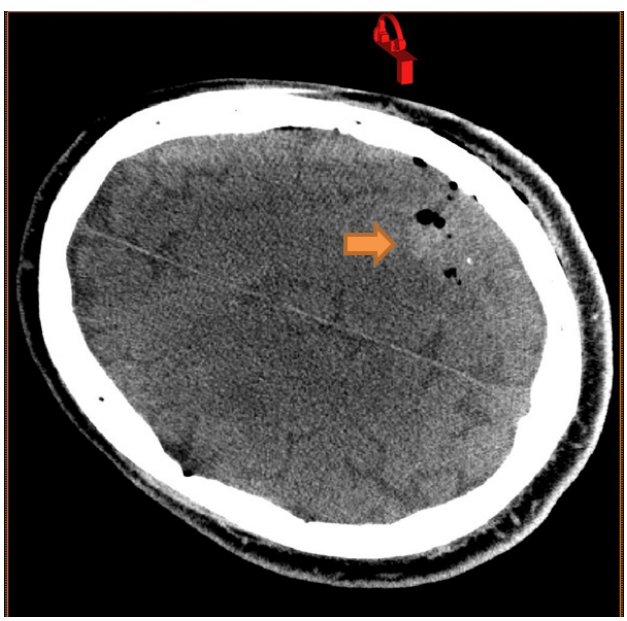

Fig. 4. Post-procedural non-contrast FDCT following biopsy needle removal. An intratumoral hemorrhage with a volume of 1.57 ml is visible at the biopsy site (orange arrow)

4–5 cores. The needle was then withdrawn after pre-injecting 2 mL of sterile saline into its lumen to visualize the sampling site by the presence of an air bubble [20]. Five minutes after needle removal, a control FDCT without additional contrast was performed. This was used to assess sampling accuracy (by the location of the gas bubble [20] (fig. 3, C), detect hemorrhage and measure its volume (fig. 4), as well as identify possible blood oozing along the biopsy tract and ventricular shift (to exclude massive intraventricular hemorrhage) (fig. 5, A–B). If hemorrhage > 1 mL was detected, rescanning was performed after 10 minutes to assess bleeding dynamics. In the absence of ongoing hemorrhage, the skin was sutured and the patient transferred to the ICU.

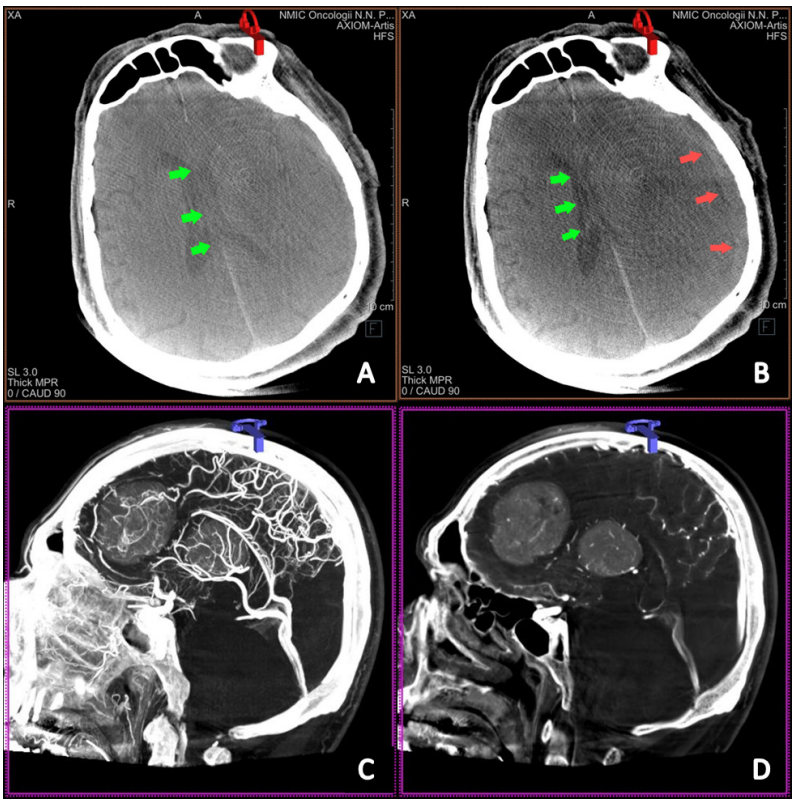

Fig. 5. A–B. Intraprocedural diagnostics of massive bleeding. A. Post-procedural non-contrast FDCT following biopsy needle removal. Displacement of cerebral midline structures is noted (green arrows); B. Second non-contrast FDCT scan 5 minutes after the initial study. Progressive midline shift is observed (green arrows) with development of a subdural hematoma (red arrows); C–D. Visualization of primary brain lymphoma using intra-arterial multiphase FDCT contrast technique. Arteriovenous (C) and parenchymal (D) phases of the study performed in the 20sDCT Head mode (high spatial resolution mode) are shown

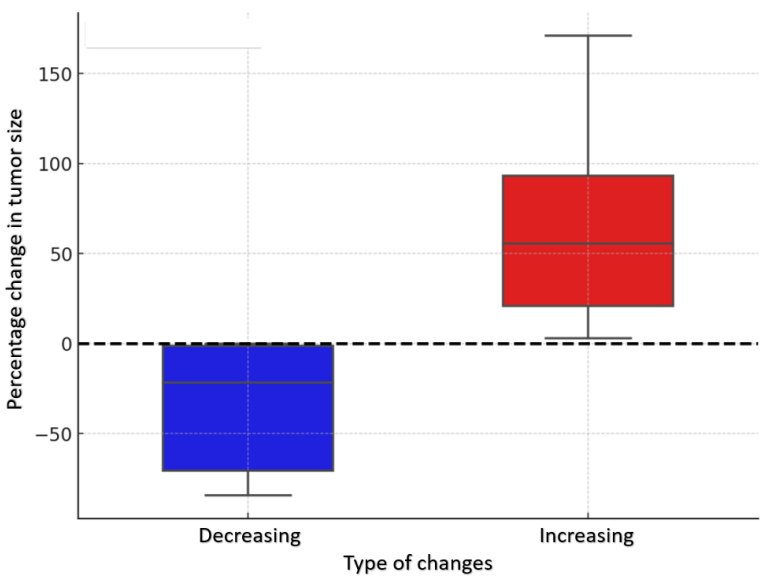

Fig. 6. Histogram showing percentage change in target tumor dimensions between preoperative imaging (MRI or PET-CT) and intraoperative FDCT with different contrast protocols

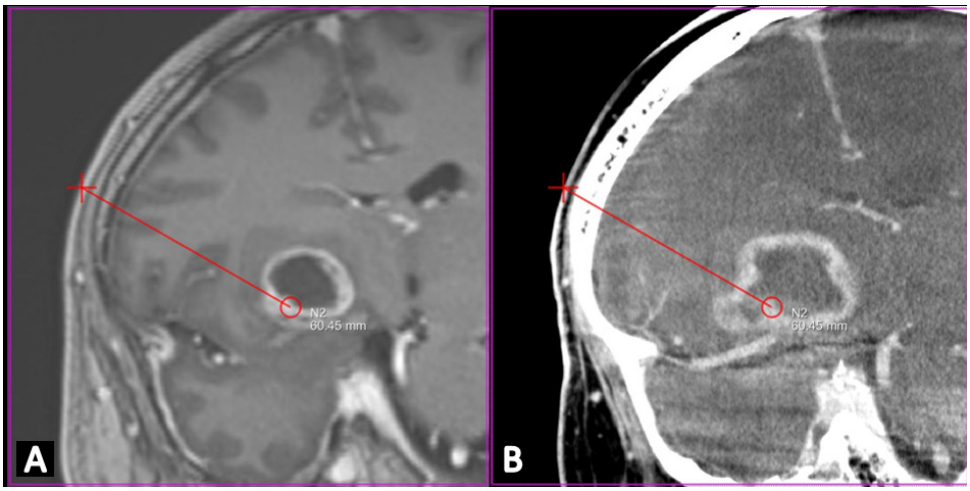

Fig. 7. Expansion of the tumor necrosis zone between preoperative MRI (A) and intraprocedural FDCT during the parenchymal phase of intravenous bolus contrast (B). The three-week interval between imaging studies demonstrates significant tumor progression. Targeting based solely on the earlier MRI would have resulted in tissue sampling from the necrotic region, likely yielding non-diagnostic histopathological results

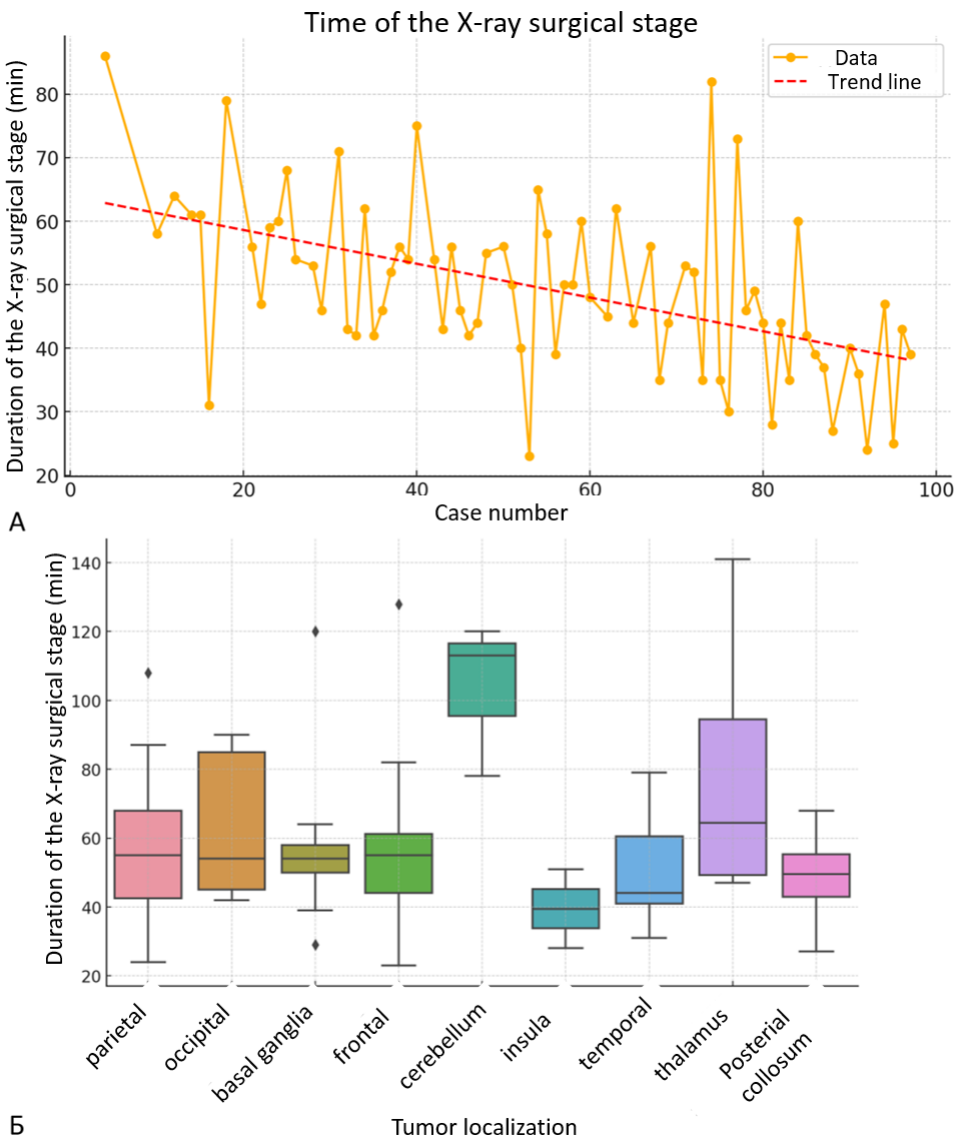

Fig. 8. A. Correlation between procedure duration for FDCT-guided stereotactic brain biopsy (STB) and operator experience (number of previously performed procedures). B. Distribution of procedure times for FDCT-guided STB according to target tumor location within the brain (see text for details)

In a subset of cases with poor tumor visualization on preoperative contrast-enhanced MRI, an intra-arterial multiphasic contrast technique was also used (fig. 5, C-D). First, via femoral access, the common carotid (or vertebral) artery on the affected side was catheterized. Then 60 mL of contrast was injected through the angiographic catheter at 2 mL/s (30-s injection), and FDCT in the 20sDCT Head mode was performed in the arteriovenous phase (scan 10 seconds after the start of injection, as described in [12]) and in the parenchymal phase (scan 10 seconds after completion of the first FDCT scan — original technique). The remaining STB steps were identical to the sequence described above for multiphasic intravenous bolus contrast administration.

Results

A total of 99 STB procedures were performed in 99 patients. FDCT-guided STB without additional contrast was used in 21 patients, intravenous contrast enhancement in 36, multiphasic intravenous enhancement in 31, and intra-arterial bolus FDCT contrast in 11, respectively. The median target tumor volume on preoperative imaging (MRI and/or PET/CT) was 6.9 mL (2.4–16.6). Target depth ranged from 13.3 to 85.2 mm; median 47.5 mm (38–56). In most cases, the target point was reached on the first needle pass; a single trajectory correction under augmented fluoroscopy was required in only 7 cases (7 %). The median number of tumor cores obtained was 5 (4–5).

During intraoperative contrast-enhanced FDCT (n = 78), a reduction in lesion volume was observed in 11 cases (14.1 %) with a median decrease of 5.0 mL (2.7–9.2), corresponding to a 34.6 % reduction from baseline tumor volume. All of these patients had received corticosteroid therapy prior to STB due to suspected primary CNS lymphoma, which was subsequently confirmed morphologically. In 46 cases (58.9 %), FDCT showed a median increase in tumor volume of 7.0 mL (2.8–14.0) compared with preoperative imaging (a 60.0 % increase from baseline) (fig. 6). Moreover, in 11 of these 46 cases, new necrotic areas or enlargement of existing necrosis and/or intratumoral hemorrhage were noted, which substantially affected trajectory planning compared with reliance on preoperative MRI and/or PET/CT (fig. 7).

On post-sampling control FDCT, the three-dimensional radial deviation from the planned targeting trajectory averaged 2.5 mm (range 0.5–3.5 mm; median 2.0 mm).

Significant brain shift after dural opening requiring substantial trajectory correction was observed in only one patient with pronounced compensatory hydrocephalus (fig. 2, C–D); minor shift not requiring correction was seen in eight patients.

The median STB procedure time was 53 minutes (43–65). With growing operator experience and staff training, procedure time decreased substantially, as reflected by the learning curve (fig. 8, A). In a post hoc analysis (Tukey HSD), Tukey's test identified significant differences in procedure duration for cerebellar lesions compared with all other tumor locations (fig. 8, B). The mean number of FDCT scans per procedure was 4 (range 3–5; median 4). The scan count depended on the contrast protocol and learning phase, as well as patient anatomy and lesion location.

Morphological and molecular-genetic verification was achieved in 97 of 99 patients (98.0 %). Diagnoses included 62 gliomas, 25 primary CNS lymphomas, five demyelinating processes, three encephalitis, one adenocarcinoma metastasis (prompting a search for the primary site), and one case of Erdheim–Chester disease. In the remaining two cases, biopsy did not yield a morphological diagnosis; however, lymphoma was verified in one patient after surgical tumor removal, and the other showed rapidly progressive disease most likely of glial origin.

Clinically significant complications occurred in 3 patients (3.0 %). Two involved intracranial hemorrhage: one due to avulsion of a bridging vein with massive subdural bleeding (fig. 5, A–B), and the other an intense intratumoral hemorrhage of 7.2 mL, which, against the background of large tumor volume and peritumoral edema, led to herniation syndrome. In both cases, emergent neurosurgical intervention was performed in the angiography suite immediately after diagnosis, achieving reliable hemostasis. A third complication — persistent hypesthesia — was related to a lesion involving the spinothalamic tract and is best considered an adverse effect of STB. Clinically insignificant intratumoral hemorrhages were detected on control FDCT in only two cases, with volumes of 0.6 mL and 1.5 mL. No seizures or infectious complications occurred. There were no deaths. On multivariable correlation analysis, no association was found between complication occurrence and tumor volume, depth, or proximity to eloquent areas (language regions, thalamus, brainstem structures, etc.). The average length of hospitalization was 4 days.

Discussion

Only two studies have previously reported clinical experience with (robotic) angiography systems equipped with FDCT — Artis Zeego (Siemens, Germany) in the first [17] and Artis Pheno (Siemens, Germany) in the second [18] — for performing STB of brain tumors. However, in both cases, FDCT scanning (without additional contrast) was

used solely to capture cranial bony landmarks for subsequent image fusion with the same preoperative MRI. Thus, in the first study, FDCT was performed with a Leksell frame affixed to the patient's head (analogous to MDCT), and standard stereotactic planning software (iPlan, Brainlab, Munich, Germany) was used for trajectory planning and STB [17]. In the second study, FDCT of the head was performed with an optical localizer mounted on a dedicated holder; this was used for coordinate registration, automatic MRI co-registration, and synchronization with the new robotic targeting system Circ (Brainlab, Munich, Germany), employed for the first time instead of the standard mechanical VarioGuide (Brainlab, Munich, Germany) used in this frameless STB variant [18].

Our prospective study demonstrated the high diagnostic effectiveness of STB using contemporary FDCT technologies. This can be attributed to the ability to continuously monitor needle position in real time, substantially improving targeting accuracy compared with "blind" placement using frame-based or optical navigation. In addition, FDCT imaging provided intraoperative, high-precision information on tumor position, volume, size, and structure, which — as shown in our work — can change rapidly (displacement, shrinkage or enlargement, development of hemorrhagic and/or necrotic areas, etc.). Moreover, when there was concern for off-target needle placement or needle-induced tumor displacement (more common when targeting metastases that often have a fibrous capsule), a repeat scan could be obtained to verify the actual needle position immediately before sampling. Two preclinical phantom studies previously demonstrated high targeting accuracy under FDCT guidance using laser navigation [21] or an optical tracking system integrated into the flat-panel detector [22]. Our clinical study, which employed both laser guidance and augmented fluoroscopy, corroborates these preliminary preclinical data.

We observed only three complications (with no deaths), supporting the high safety of FDCT-guided STB. It should be noted that serious complications and mortality, as previously shown, are almost entirely attributable to intraprocedural hemorrhage [23], which becomes clinically apparent within the first hour after sampling in half of cases and within the first 6 hours in three quarters (median 60 minutes) [24]. The FDCT-based visualization workflow we propose enables the earliest (intraoperative) diagnosis of subclinical intratumoral hemorrhage and other bleeding types, and allows immediate surgical management directly in the interventional radiology suite where STB is performed (e.g., placement of an external ventricular drain or hematoma drainage). This undoubtedly further enhances the safety of the STB procedure.

Another clear advantage of the proposed method is its high degree of technical integration, which streamlines the entire workflow and mitigates the time and economic costs associated with involving diagnostic radiology departments.

Given that interventional radiology suites equipped with modern angiography systems capable of FDCT are available in virtually all oncology centers and dispensaries, this method may prove in demand for the verification of primary and metastatic brain tumors.

We did not specifically quantify radiation dose to staff and patients during FDCT-guided STB. Nevertheless, considerations can be drawn from published FDCT dose metrics. A head-and-neck phantom study showed that doses with FDCT are at least twofold lower than during a single-phase MDCT scan [25]. In our series, patients underwent an average of four FDCT scans, which is comparable to one biphasic MDCT of the head. Considering that our technique largely obviates MDCT both at the preoperative planning stage and for assessing intratumoral hemorrhage and other complications, one can argue that the total radiation dose during FDCT-guided biopsy is comparable to — or up to twice lower than — that during frame-based STB. Moreover, it is well known that, owing to its arc trajectory, FDCT reduces ocular (lens) dose by more than fivefold compared with ring-trajectory MDCT [25]. In routine practice, the number of FDCT scans can be further reduced if MRI and/or PET/CT fusion is used for navigation; in such cases FDCT can be performed in substantially lower-dose "bone" modes sufficient to capture these highly informative modalities [10, 25]. The trade-off, however, is a potential increase in the risk of serious complications alongside reduced diagnostic effectiveness. In any case, after optimizing the FDCT-guided STB algorithm, studies assessing radiation exposure to both patients and staff are warranted. Randomized trials comparing the diagnostic yield and safety of our FDCT-guided approach with frame-based and optical STB are also advisable. A promising direction is the integration of optical and electromagnetic tracking technologies, together with robotic targeting, into existing angiography suites, which may reduce radiation while preserving the high diagnostic effectiveness of the proposed STB method [9].

In conclusion, our study demonstrates the high diagnostic effectiveness and safety of FDCT-guided STB for brain tumors. The proposed method mitigates the principal limitations of frame-based and frameless STB by enabling reliable intraoperative trajectory planning, high-quality real-time neuroimaging and neuronavigation, and intraoperative diagnosis of potential complications with timely management. This STB technique appears

highly promising for broader clinical adoption, particularly in oncology institutions that already house neuro-oncology services and interventional radiology units. Further development of this area of interventional neuro-oncology is also feasible within new hybrid neurosurgical operating rooms equipped with modern robotic angiography systems.

Conflict of interests
The authors declare no conflict of interest.
Funding
This study was performed without funding.
Compliance with patient rights and principles of bioethics
The study was conducted in accordance with the Declaration of Helsinki (2013). For this type of study, formal approval from an institutional ethics committee was not required.
Authors' contributions
Kurnosov I.A., Balakhnin P.V.: Study design and conceptualization, data collection, literature review and analysis, manuscript drafting.
Gulyaev D.A., Subbotina D.R., Malkevich V.I.: Study design and conceptualization, manuscript drafting.
Muravtseva A.L., Shmelev A.S., Chirkin V.Yu., Burovik I.A.: Literature review and analysis, critical revision and scientific editing of the manuscript.
Bagnenko S.S., Belyaev A.M.: scientific editing of the manuscript.
All authors approved the final version of the article prior to publication and agreed to take responsibility for all aspects of the work, including the proper review and resolution of any issues related to its accuracy or integrity.

REFERENCES

1. Patel K.S., Carter B.S., Chen C.C. Role of biopsies in the management of intracranial gliomas. *Prog Neurol Surg*. 2018; 30: 232-243.-DOI: https://doi.org/10.1159/000464439.
2. Callovini G.M., Telera S., Sherkat S., et al. How is stereotactic brain biopsy evolving? A multicentric analysis of a series of 421 cases treated in Rome over the last sixteen years. *Clin Neurol Neurosurg*. 2018; 174: 101-107.-DOI: https://doi.org/10.1016/j.clineuro.2018.09.020.
3. Yu K.K.H., Patel A.R., Moss N.S. The role of stereotactic biopsy in brain metastases. *Neurosurg Clin N Am*. 2020; 31(4): 515-526.-DOI: https://doi.org/10.1016/j.nec.2020.06.002.
4. Dhawan S., He Y., Bartek J., et al. Comparison of frame-based versus frameless intracranial stereotactic biopsy: Systematic review and meta-analysis. *World Neurosurg*. 2019; 127: 607-616.e4.-DOI: https://doi.org/10.1016/j.wneu.2019.04.016.
5. Maryashev S.A., Poddubskiy A.A., Pronin I.N., et al. MRI imaging for planning stereotactic biopsies of the brain lesions. *Medicinskaâ vizualizaciâ=Medical Visualization.* 2022; 26(2): 18-38.-EDN: JHODOR.-DOI: https://doi.org/10.24835/1607-0763-1046 (in Rus).
6. Ungar L., Nachum O., Zibly Z., et al. Comparison of frame-based versus frameless image-guided intracranial stereotactic brain biopsy: A retrospective analysis of safety and efficacy. *World Neurosurg*. 2022; 164: e1-e7.-DOI: https://doi.org/10.1016/j.wneu.2021.07.063.
7. Sugii N., Matsuda M., Tsurubuchi T., Ishikawa E. Hemorrhagic complications after brain tumor biopsy: Risk-reduction strategies based on safer biopsy targets and techniques. *World Neurosurg*. 2023; 176: e254-e264.-DOI: https://doi.org/10.1016/j.wneu.2023.05.046.
8. Bex A., Mathon B. Advances, technological innovations, and future prospects in stereotactic brain biopsies. *Neurosurg Rev*. 2022; 46(1): 5.-DOI: https://doi.org/10.1007/s10143-022-01918-w.
9. Balakhnin P.V., Burovik I.A., Bagnenko S.S. Technologies of visualization, guidance and tracking in interventional oncology: Current capabilities and prospects for further development. *Medicina Vysokih Tehnologij*. 2024; 2(2): 5-21.-EDN: CHVTFU (in Rus).
10. Kalender W.A., Kyriakou Y. Flat-detector computed tomography (FD-CT). *Eur Radiol*. 2007; 17(11): 2767-79.-DOI: https://doi.org/10.1007/s00330-007-0651-9.
11. Balakhnin P.V., Bagnenko S.S., Belyaev A.M. Flat-detector computed tomography in interventional radiology: Background and history of creation. *Medicina Vysokih Tehnologij*. 2024; 2(1): 12-34.-EDN: GKYDDI (in Rus).
12. Raz E., Nossek E., Sahlein D.H., et al. Principles, techniques and applications of high resolution cone beam CT angiography in the neuroangio suite. *J Neurointerv Surg*. 2023; 15(6): 600-607.-DOI: https://doi.org/10.1136/jnis-2022-018722.
13. Key B.M., Tutton S.M., Scheidt M.J. Cone-beam CT with enhanced needle guidance and augmented fluoroscopy overlay: Applications in interventional radiology. *AJR Am J Roentgenol*. 2023; 221(1): 92-101.-DOI: https://doi.org/10.2214/AJR.22.28712.
14. Cooke D.L., Levitt M., Kim L.J., et al. Transcranial access using fluoroscopic flat panel detector CT navigation. *AJNR Am J Neuroradiol*. 2011; 32(4): E69-70.-DOI: https://doi.org/10.3174/ajnr.A2066.
15. Fiorella D., Peeling L., Denice C.M., et al. Integrated flat detector CT and live fluoroscopic-guided external ventricular drain placement within the neuroangiography suite. *J Neurointerv Surg*. 2014; 6(6): 457-60.-DOI: https://doi.org/10.1136/neurintsurg-2013-010856.
16. Yang Z., Hong B., Jia Z., et al. Treatment of supratentorial spontaneous intracerebral hemorrhage using image-guided minimally invasive surgery: Initial experiences of a flat detector CT-based puncture planning and navigation system in the angiographic suite. *AJNR Am J Neuroradiol*. 2014; 35(11): 2170-5.-DOI: https://doi.org/10.3174/ajnr.A4009.
17. Enders F., Rothfuss A., Brehmer S., et al. Optimized intraoperative imaging for stereotactic planning with a multiaxial robotic C-arm system: Technical note and case series. *J Neurol Surg A Cent Eur Neurosurg*. 2022; 83(6): 588-595.-DOI: https://doi.org/10.1055/s-0041-1731754.
18. Truckenmueller P., Früh A., Kissner J.F., et al. Integration of a lightweight and table-mounted robotic alignment tool with automated patient-to-image registration using robotic cone-beam CT for intracranial biopsies and stereotactic electroencephalography. *Neurosurg Focus*. 2024; 57(6): E2.-DOI: https://doi.org/10.3171/2024.9.FOCUS24525.
19. Kurnosov I.A., Balakhnin P.V., Subbotina D.R., et al. Intraoperative flat-panel computed tomography as the method of choice for stereotactic biopsy of brain tumors. *Voprosy Onkologii = Problems in Oncology*. 2023; 69(3S): 287-288.-EDN: SVIIID (in Rus).
20. Poca M.A., Martínez-Ricarte F-R., Gándara D.F., et al. Target location after deep cerebral biopsies using low-volume air injection in 75 patients. Results and technical note. *Acta Neurochir (Wien)*. 2017; 159(10): 1939-1946.-DOI: https://doi.org/10.1007/s00701-017-3191-3.

21. Mabray M.C., Datta S., Lillaney P.V., et al. Accuracy of flat panel detector CT with integrated navigational software with and without MR fusion for single-pass needle placement. *J Neurointerv Surg*. 2016; 8(7): 731-5.-DOI: https://doi.org/10.1136/neurintsurg-2015-011799.
22. Skyrman S., Lai M., Edström E., et al. Augmented reality navigation for cranial biopsy and external ventricular drain insertion. *Neurosurg Focus*. 2021; 51(2): E7.-DOI: https://doi.org/10.3171/2021.5.FOCUS20813.
23. Riche M., Amelot A., Peyre M., et al. Complications after frame-based stereotactic brain biopsy: a systematic review. *Neurosurg Rev*. 2021; 44(1): 301-307.-DOI: https://doi.org/10.1007/s10143-019-01234-w.
24. Riche M., Marijon P., Amelot A., et al. Severity, timeline, and management of complications after stereotactic brain biopsy. *J Neurosurg*. 2021; 136(3): 867-876.-DOI: https://doi.org/10.3171/2021.3.JNS21134.
25. Daly M.J., Siewerdsen J.H., Moseley D.J., et al. Intraoperative cone-beam CT for guidance of head and neck surgery: Assessment of dose and image quality using a C-arm prototype. *Med Phys*. 2006; 33(10): 3767-80.-DOI: https://doi.org/10.1118/1.2349687.

Received / 14.04.2025
Reviewed / 27.07.2025
Accepted for publication / 25.09.2025

About the authors / ORCID

Ivan A. Kurnosov / ORCID ID: https://orcid.org/0000-0003-2857-8368; eLibrary SPIN: 9131-7381; Author ID: 1065892.

Pavel V. Balakhnin / ORCID ID: https://orcid.org/0000-0002-3042-6729; eLibrary SPIN: 1431-4012; Author ID: 727661.

Dmitry A. Gulyaev / ORCID ID: https://orcid.org/0000-0002-5509-5612; eLibrary SPIN: 1612-8261; Author ID: 305822.

Daria R. Subbotina / ORCID ID: https://orcid.org/0000-0003-0836-4960; eLibrary SPIN: 8244-1435; Author ID: 1136236.

Vasilii I. Malkevich / ORCID ID: https://orcid.org/0000-0002-1082-6071; eLibrary SPIN: 8143-9671; Author ID: 988405.

Anastasia L. Muravtseva / ORCID ID: https://orcid.org/0000-0002-4221-4248; eLibrary SPIN: 9412-0279; Author ID: 1118320.

Aleksei S. Shmelev / ORCID ID: https://orcid.org/0000-0002-1610-8820; eLibrary SPIN: 2772-2824; Author ID: 860525.

Vladislav Yu. Chirkin / ORCID ID: https://orcid.org/0000-0002-0610-1131; eLibrary SPIN: 2940-3562; Author ID: 474360.

Ilya A. Burovik / ORCID ID: https://orcid.org/0000-0002-4714-1228; eLibrary SPIN: 1923-6457; Author ID: 972194.

Sergey S. Bagnenko / ORCID ID: https://orcid.org/0000-0002-4131-6293; eLibrary SPIN: 4389-9374; Author ID: 779096.

Aleksey M. Belyaev / ORCID ID: https://orcid.org/0000-0001-5580-4821; eLibrary SPIN: 9445-9473; Author ID (Scopus): 273109.